Effect of ion beam assisted deposition on the growth of indium tin oxide (ITO) nanowires

Hak Ki Yu† and Jong-Lam Lee*

We developed a method to control the alignment and density of indium tin oxide (ITO) nanowires by using ion beam assisted deposition (IBAD). During electron beam evaporation, IBAD changed the randomly oriented branch type nanowires to aligned nanowires without branches. This is due to the energetic ion beams which play a role in nucleating tin containing indium nanodots at the initial stage of growth. The improved alignment of the ITO nanowires reduced the sensing time for ethanol gas.

Indium tin oxide (ITO: Sn doped In_2O_3) has been studied extensively in the optoelectronic industry because of its unique transparent and conducting properties.[1–3] Some of its disadvantages, such as the high cost of indium and the brittleness of the oxide itself, have been overcome by modern technologies (indium recycling and nanostructure fabrication).[4,5] Therefore, ITO has remained one of the most important transparent conducting materials. Moreover, uniform ITO nanostructures provide a higher surface to volume ratio and crystallinity than polycrystalline films which are essential in producing highly efficient devices.

Typically, ITO nanowires can be produced by methods such as chemical vapor deposition,[6–8] pulsed laser deposition,[9] electrospinning,[10] *etc.* However, these synthetic methods use a metal catalyst such as Au or a self-catalytic (indium–tin) nanodot for the vapor–liquid–solid (VLS) process. In both cases, the substrate is heated to more than 800 °C to maintain the liquid Au phase and the carbothermal reaction (mixing In_2O_3 and SnO_2 powders with graphite powder to make a pure indium–tin metal catalyst for the VLS process)[7,8] between graphite powder and In_2O_3 and SnO_2. Moreover, the by-products induced by Au and graphite, such as AuIn, $AuIn_2$, and metal carbonate, can degrade the quality

Department of Materials Science and Engineering and Division of Advanced Materials Science, Pohang University of Science and Technology (POSTECH), Pohang, 790-784, South Korea. E-mail: jllee@postech.ac.kr; Fax: +82 54 279 5242; Tel: +82 54 279 2152

† Present Address: Max-Planck-Institut Für Biophysikalische Chemie, am Fassberg 11, 37077, Göttingen, Germany.
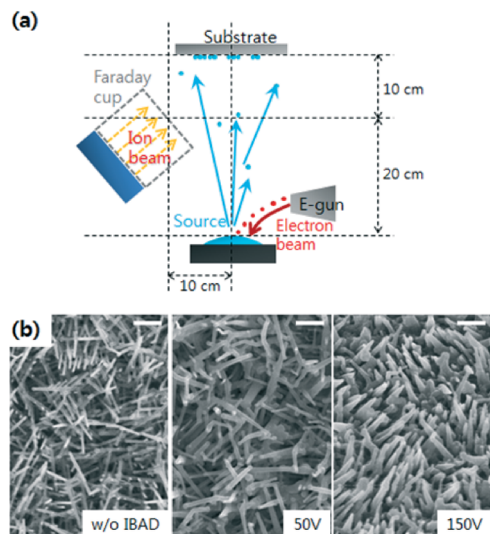
of the ITO nanostructures.[11] Meanwhile, electron beam deposition based on the self-catalytic VLS process is the most attractive method for growing ITO nanowires of large area uniformity at low temperatures below 150 °C, which a conventional polymer material can tolerate.[5,11] Although electron beam deposition may be able to control the large area uniformity of ITO nanowires, it cannot easily control their density or alignment. Because the physics (light tracing, current flow, and gas dynamics in 3-dimensional nanostructures) of ITO nanowire applied devices strongly depends on the density and alignment of ITO nanowires, it is important to develop a method to control the growth of ITO nanowires during electron beam deposition. Meanwhile, ion beam assisted deposition (IBAD) has been widely used to control the orientation or density of thin films.[12,13] If we apply IBAD to the ITO nanowire growth, the high energy particle beam can modulate the heterogeneous nucleation of the catalyst for the VLS growth of ITO nanowires. In addition, the electrical force between the charged particle beam and the evaporated materials will affect the alignment of the nanowires.

In this work, we developed a method using IBAD to control the density and alignment of ITO nanowires grown by electron beam deposition. During electron beam deposition, the energetic ion particles continuously collided with evaporated materials and adsorbed adatoms, as shown in Fig. 1a, resulting in different types of ITO nanowires from the branch-type to the partially aligned-type. These ITO nanowires were applied as gas sensors and their chemisorption and desorption dynamics were compared, especially in terms of their response speed to ethanol vapor at room temperature.

An n-type (100) silicon substrate (doped with arsenic) covered by 150 nm thick thermal oxide was used as a starting substrate. The substrate was cleaned with acetone, ethyl alcohol, and deionized water. The ITO nanowires were fabricated using the electron beam deposition method. A tin doped (10%) indium oxide pellet (purity: 99.99%) was used as the source material. The ITO nanowires were grown at a rate of

Fig. 1 (a) Schematic of the IBAD system. (b) 45° tilted SEM images of ITO nanostructures with respect to the ion beam intensity of 0 to 150 V. The beam current was set at 0.2 mA cm^{-2}. Scale bar, 200 nm.

0.5 nm s^{-1}. The chamber pressure was maintained at approximately 10^{-5} Torr during deposition and the substrate temperature was held at 300 °C to obtain well-developed ITO nanowires.[11] For IBAD, nitrogen (N$_2$) gas was introduced into the chamber, and the gas pressure was set to 0.2 mTorr. The ion beam voltage was modulated from 0 to 150 V, and the emission current was set to 0.2 mA cm^{-2}. Scanning electron microscopy (SEM) using a PHILIPS XL30S was carried out at an acceleration voltage of 10 kV and a working distance of 5 mm. Scanning Auger Microscopy (SAM) was carried out using a ULVAC PHI700, VG 310F, which has a 7 nm minimum beam size and 0.5% element detection sensitivity. X-ray photoemission spectroscopy (XPS) was performed at the 4B1 beam line at Pohang Accelerator Laboratory (PAL). An incident photon energy of 630 eV was used to obtain In 3d and Sn 3d core level spectra. High-resolution X-ray diffraction (XRD) using synchrotron radiation was performed at the 3C2 beam line at PAL. High-resolution transmission electron microscopy (HRTEM) images were taken using a Cs-corrected JEM 2200FS operated at 200 kV. Gas sensor devices which adopted the ITO nanowires were fabricated, as described below. Soda-lime glass (2 cm × 2 cm) was used as the starting substrate. The glass was cleaned sequentially with acetone, ethyl alcohol, and deionized water. After the growth of ITO nanowires on the substrate, Cr/Au (50 nm/200 nm) pad electrodes of 2 mm × 2 mm size were deposited on the nanostructures. The concentrations of ethanol gas of about 1000 ppm and 2000 ppm were calibrated by a conventional gas sensor, and gas of each concentration was injected by a mass flow controller onto the top of the devices. The *I–V* changes based on the amount of gas adsorption/desorption were measured in ambient air at room temperature using a Keithley 2400 source measurement unit.

Fig. 1b shows the 45° tilted-view SEM images of ITO nanowires grown for 300 s with respect to the ion beam voltage intensity (emission current was set constant at 0.2 mA). The branch-type ITO nanowires (synthesized under normal electron beam evaporation conditions) gradually disappeared with the increase of the ion beam voltage from 50 V to 150 V. To compare these morphological differences, we studied the early stage of ITO nanowire growth. The inset SEM image in Fig. 2a shows the ITO surface grown by normal electron beam deposition just for 20 s. Nano-sized droplets were distributed for the VLS process. The detailed composition of the droplets was confirmed by Auger spectroscopy (spot 1: droplet region, spot 2: base region), as shown in Fig. 2a. The significant difference in the Auger spectra is the tin concentration (spot 1 has 43% higher tin concentration than spot 2). The relatively high composition of tin promoted the formation of tin doped indium nano-sized droplets due to the low melting point of the eutectic In(Sn) alloy (eutectic point atomic concentration: 52% indium and 48% tin).[14] Moreover, the higher diffusivity of tin (~2.6 × 10^{-18} cm^2 s^{-1}) compared to indium (~2.3 × 10^{-18} cm^2 s^{-1}) in the In(Sn) alloy promoted this phenomenon.[15] The effect of IBAD on the activity of tin during ITO evaporation could be determined by XPS measurements with respect to growth time. Fig. 2b shows the In and Sn 3d core level spectra of the ITO samples grown for 20 s with and without IBAD. The samples grown by IBAD showed about half the tin concentration of samples grown by the normal electron beam deposition method. This means that IBAD can strongly reduce the density of In(Sn) nanodots for VLS growth, as shown in the inset SEM image of Fig. 2b. As shown in Fig. 2c (Sn 3d to In 3d ratios: these ratios were corrected by the XPS sensitivity factor; Sn 3d 5/2: 5.176 and
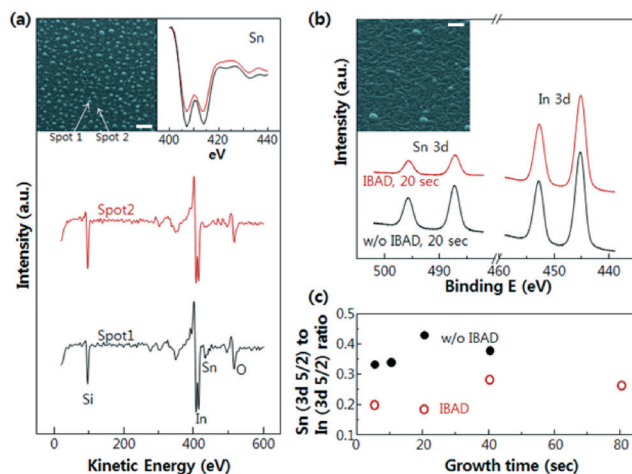

Fig. 2 (a) Auger spectra of spots 1 and 2 in the inset. The inset is a 45° tilted SEM image of the initial stage of ITO nanowire growth (for 20 s without IBAD). Scale bar, 100 nm. The enlarged graph is the Sn spectra of spots 1 and 2. (b) In and Sn 3d XPS core level spectra of ITO nanowires grown for 20 s. The inset is a 45° tilted SEM image of the initial stage of ITO nanowire growth (for 20 s of IBAD). Scale bar, 100 nm. (c) The Sn (3d 5/2) to In (3d 5/2) ratio of ITO nanowires with respect to growth time.

In 3d 5/2: 4.359),[16] this tendency is the same in the entire range of growth times from 5 s to 40 s. As the growth time increased, the ratio slightly decreased due to the development of ITO nanowires from In(Sn) nanodots.

Under normal electron beam evaporation conditions, branch-type ITO nanowires developed with time (Fig. 3a). The metallic In(Sn) nanodots, shown in the 20 second growth image, initiated the VLS process, resulting in ITO nanowires. ITO branches were developed by the additional nucleation of In(Sn) nanodots on the (100) family plane of the bixbyite ITO crystal.

However, the growth of ITO nanowires synthesized with and without IBAD (under 150 V, 0.2 mA conditions) significantly differed, as shown in Fig. 3a. The nucleation of In(Sn) nanodots was suppressed by IBAD because the energetic ion beam blocked the migration of adatoms, especially Sn. This blockage promoted the formation of nanodots through the reduction of the melting point of the eutectic In(Sn) alloy. Moreover, the ion beam also blocked the additional nucleation of In(Sn) nanodots on the (100) family plane of ITO, resulting in nanowires without any branches, as shown in the 300 s growth image. The aligned ITO nanowires synthesized by IBAD could be understood as the result of electrical repulsion between individual nanowires during growth due to the formation of electrostatic forces by IBAD.[17,18] The self-bias

potential established on the immersed substrate surface in the ion plasma environment makes the electric field lines which are invariably terminated perpendicular to the surface.[18] The electrostatic forces would force these one-dimensional nanostructures to align with the field direction, an energetically most favorable orientation. Because the (100) orientation of the bixbyite ITO crystal is unstable due to polarity, there is a strong tendency for the crystal to have a reconstructed surface such as the (111) facet,[19] resulting in tilt alignment from the surface normal of about 54.7° as shown in the inset of Fig. 3a. Each ITO nanowire was aligned in the bixbyite single crystal In_2O_3 (100) orientation with 0.506 nm spacing (Fig. 3b); this orientation was confirmed by a normal θ–2θ scan, as shown in Fig. 3c. The ITO nanowires grown by normal electron beam evaporation gave an XRD pattern with a random orientation, showing all possible diffraction lines due to the randomly distributed (100) orientation of the branch structure. On the other hand, the ITO nanowires grown by IBAD showed a relatively strong (222) diffraction peak. This peak means that the ITO nanowires with the (100) growth orientation were aligned in the (111) direction at a 54.7° tilt angle.

We applied these ITO nanowires as gas sensors and compared their chemisorption and desorption dynamics, especially in terms of their response speed to ethanol vapor at room temperature, as shown in Fig. 4b. Basically, the initial resistance of the ITO nanobranches (~78 Ω) was lower than that of the IBAD ITO nanowires (~115 Ω) by about 32% due to the many connections among the ITO nanowires (Fig. 4a). The mechanism responsible for the difference in resistance can be explained as follows. When the ITO nanowires were exposed to air, oxygen molecules chemisorbed onto the surface of the nanowires and captured electrons from the nanowires, making the nanowires less conductive. When the nanowires were exposed to a reducing gas such as ethanol vapor, the ethanol molecules reacted with the oxygen ions and released the electrons back into the conduction channel, thereby reducing the resistance of the ITO nanowires.[20,21] There is a significant difference in the response time of the chemisorption–desorption process between the ITO nanobranches and the IBAD nanowires. The IBAD ITO nanowires showed a faster response time of about 1.5–2 s than the ITO nanobranches, which showed a response time of about 12–15 s. The resistance fluctuations of the IBAD ITO nanowires after exposure to ethanol were due to the interference of gas molecules between the reacted out-diffusion gas and the unreacted in-diffusion gas. Although ITO nanobranches also showed resistance fluctuations, the frequency of the fluctuations was significantly lower than that of the IBAD ITO nanowires due to the lower out-diffusion and in-diffusion speeds of gas molecules through the dense branch structure. Similarly, the two devices showed different recovery times: 3–5 s for the IBAD ITO nanowires and ~40 s for the ITO nanobranches. There are two possible dynamic routes for oxygen molecules; one is physical scattering, resulting in loss of energy as phonons of solid surfaces and the other is the
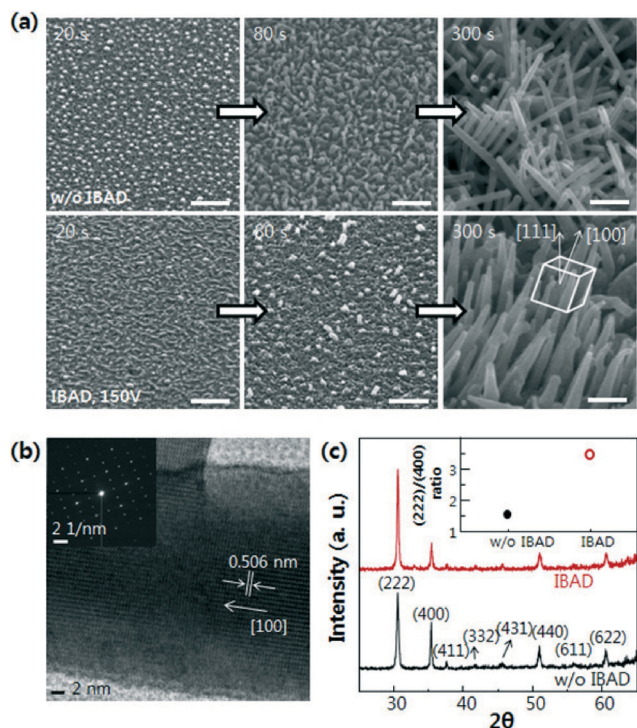

Fig. 3 (a) 45° tilted SEM images of ITO nanowires with respect to growth time from 20 s to 300 s. The schematic inset shows the (111) q_z diffraction of the (100) aligned cubic system. Scale bar, 100 nm. (b) The high resolution TEM image and the diffraction pattern of ITO nanowires grown by normal electron beam evaporation for 300 s. (c) The X-ray diffraction pattern of ITO nanowires grown for 300 s. The inset is the intensity ratio of (222)/(400) peaks.
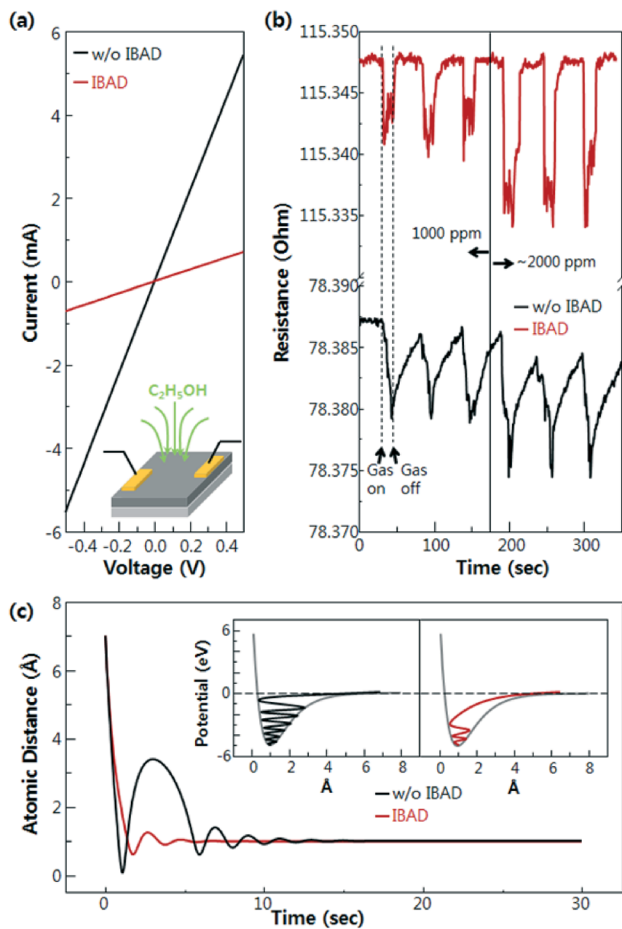
Fig. 4 The *I–V* curve of the Cr/Au contact pad on ITO nanowires. (b) Resistance changes of ITO nanowires with respect to the repeated gas-on and gas-off operation and concentration. (c) Simulated trajectories of the oxygen molecule for chemisorption on ITO nanowire surfaces following the Morse potential. The inset is the schematics of the trajectory motions on the Morse potential curve.

re-chemisorption and re-desorption loop in the nanostructure matrix. For the physical scattering route, the surface morphology of the nanostructures is very important and the aligned nanorods by IBAD have advantages for the fast translation of oxygen molecules compared to the complex nanobranches. For the chemisorption–desorption loop route, we can focus on the trajectories of gas molecules during the chemisorption process based on the Morse potential defined as $V(r) = D[1 - \exp\{-a(r - r_e)\}]^2 - D$, where $V(r)$ is the potential energy with respect to the atomic distance r, D is the potential depth at the equilibrium bond distance r_e, and a is defined as $(k/2D)^{1/2}$ where k is the spring constant.[22] In this potential curve, the first derivative is the acceleration of a gas molecule that approaches the specific surface. It needs some friction to attach (chemisorption) the gas molecule onto a specific solid surface, otherwise, the gas molecule will be easily scattered due to strong negative acceleration at the repulsion potential line (near the surface). In this sense, the aligned ITO nanorods synthesized by IBAD could have a larger friction coefficient than the nanobranches because the friction coefficient

strongly depends on the surface states such as point defects and depleted charges formed by the energetic ion beam, resulting in fast chemisorption of oxygen molecules.[23] We can simply simulate the trajectories of the oxygen gas molecule by assuming some variables in the Morse potential; D is about 5 eV for general chemisorption on an oxide surface, r_e is about 1 Å, a is about 1 Å^{-1}.[24] If we assume the friction coefficient to be 1.5 for IBAD ITO nanorods and 0.8 for ITO nanobranches, the trajectories of gas molecules could be calculated as shown in Fig. 4c. The oxygen molecule on ITO nanobranches shows multiple vibration paths in the potential wall while that on IBAD ITO nanorods shows a small number of vibrations in the potential wall. So, the origin of the fast response time in IBAD ITO nanorods could be understood as: i) fast translation of the gas molecule without multiple physical scattering in the nanostructure matrix due to alignment; and ii) fast chemisorption of oxygen gas due to the large friction originating from defects at the surface. We also have to think about the formation of nitrides such as InN during IBAD. However, there was no nitride detected in crystallographic measurements such as XRD and TEM. Moreover, we also checked the N 1s spectra during XPS measurements; however, there was no nitrogen signal at all. Because the Gibbs free energy change for formation of In_2O_3 (-765.57 kJ mol^{-1} at 500 K) is much lower than that of InN (-103.60 kJ mol^{-1} at 500 K),[25] it is very difficult for that kind of nitride formation to happen.

In this work, the effect of IBAD on the growth of ITO nanowires was studied. During electron beam evaporation, IBAD and its energetic ion beam changed the In(Sn) nanodot nucleation process and thus changed randomly oriented branch-type nanowires to relatively well-aligned paralleled nanowires. The alignment of ITO nanowires significantly affected the response time of the ITO gas sensor, especially when ethanol gas was used. This alignment and density control technique will be used to improve the performance of devices using ITO nanowires.

Acknowledgements

References

1 Y. Park, V. Choong, Y. Gao, B. R. Hsieh and C. W. Tang, *Appl. Phys. Lett.*, 1996, **68**, 2699.
2 M. G. Mason, L. S. Hung, C. W. Tang, S. T. Lee, K. W. Wong and M. Wang, *J. Appl. Phys.*, 1999, **86**, 1688.

3   T. Margalith, O. Buchinsky, D. A. Cohen, A. C. Abare, M. Hansen, S. P. DenBaars and L. A. Coldren, *Appl. Phys. Lett.*, 1999, **74**, 3930.

4   S.-J. Hsieh, C.-C. Chen and W. C. Say, *Mater. Sci. Eng., B*, 2009, **158**, 82.

5   H. K. Yu, S. Kim, B. Koo, G. H. Jung, B. Lee, J. Ham and J.-L. Lee, *Nanoscale*, 2012, **4**, 6831.

6   Q. Wan, E. N. Dattoli, W. Y. Fung, W. Guo, Y. Chen, X. Pan and W. Lu, *Nano Lett.*, 2006, **6**, 2909.

7   X. Y. Xue, Y. J. Chen, Y. G. Liu, S. L. Shi, Y. G. Wang and T. H. Wang, *Appl. Phys. Lett.*, 2006, **88**, 201907.

8   A. J. Chiquito, A. J. C. Lanfredi and E. R. Leite, *J. Phys. D: Appl. Phys.*, 2008, **41**, 045106.

9   R. Savu and E. Joanni, *Scr. Mater.*, 2006, **55**, 979.

10 M. M. Munir, F. Iskandar, K. M. Yun, K. Okuyama and M. Abdullah, *Nanotechnology*, 2008, **19**, 145603.

11 H. K. Yu, W. J. Dong, G. H. Jung and J.-L. Lee, *ACS Nano*, 2011, **5**, 8026.

12 C. P. Wang, K. B. Do, M. R. Beasley, T. H. Geballe and R. H. Hammond, *Appl. Phys. Lett.*, 1997, **71**, 2955.

13 L. Dong and D. J. Srolovitz, *Appl. Phys. Lett.*, 1999, **75**, 584.

14 H. Okamoto, *J. Phase Equilib. Diffus.*, 2004, **27**, 313.

15 J. P. Daghfal and J. K. Shang, *J. Electron. Mater.*, 2007, **36**, 1372.

16 D. Briggs and M. P. Seah, *Practical Surface Analysis by Auger and X-Ray Photoelectron Spectroscopy*, Wiley, New York, 1983.

17 W. Ahmed, E. S. Kooij, A. van Silfhout and B. Poelsema, *Nano Lett.*, 2009, **9**, 3786.

18 C. Bower, W. Zhu, S. Jin and O. Zhou, *Appl. Phys. Lett.*, 2000, **77**, 830.

19 E. H. Morales and U. Diebold, *Appl. Phys. Lett.*, 2009, **95**, 253105.

20 J.-H. Lee, *Sens. Actuators, B*, 2009, **140**, 319.

21 N. Yamazoe, *Sens. Actuators, B*, 2005, **108**, 2.

22 E. Shustorovich, *Surf. Sci. Rep.*, 1986, **6**, 1.

23 W. Ahmed, E. S. Kooij, A. van Silfhout and B. Poelsema, *Nano Lett.*, 2009, **9**, 3786.

24 Y. D. Kim, A. P. Seitsonen, S. Wendt, J. Wang, C. Fan, K. Jacobi, H. Over and G. Ertl, *J. Phys. Chem. B*, 2001, **105**, 3752.

25 I. Barin, *Thermochemical Data of Pure Substances*, Wiley, New York, 1989.